sustainability

MDPI

Article

Effect of CO_2 Mineralization on the Composition of Alkali-Activated Backfill Material with Different Coal-Based Solid Wastes

Binbin Huo [1], Jixiong Zhang [1,*], Meng Li [2], Nan Zhou [1], Xincai Qiu [3], Kun Fang [1,*] and Xiao Wang [1]

1 School of Mines, China University of Mining and Technology, Xuzhou 221116, China; huobinbin@cumt.edu.cn (B.H.); zhounanyou@126.com (N.Z.); x.wang@cumt.edu.cn (X.W.)
2 State Key Laboratory of Coal Resources and Safe Mining, China University of Mining and Technology, Xuzhou 221116, China; limeng77521@126.com
3 Jining Energy Bureau, Jining 272067, China; jnsnyjmtk@163.com
* Correspondence: cumtzjxiong@163.com (J.Z.); fangkun0918@cumt.edu.cn (K.F.)

Abstract: Research focusing on waste management and CO_2 mineralization simultaneously has been a popular topic in the mining community, and a common approach is to mineralize CO_2 with coal-based solid waste (CSW, e.g., gangue (CG), fly ash (FA), coal gasification slag (CGS)) produced by mining activities. Despite the understanding of CO_2 mineralization by cementitious materials, the mineralization capacity of alkali-activated CSWs remains unknown. Therefore, the mineral composition evolution and mineralization capacity of different alkali-activated materials (prepared with CG, FA, CGS, and sodium hydroxide (which works as the alkali-activator), respectively) are investigated with the adoption of Gibbs Energy Minimization Software (GEMS). The results indicate that the abovementioned three alkali-activated CSWs are majorly composed of calcium silicate hydrate, magnesium silicate hydrate, kaolinite, sodium zeolite, and liquid. Due to the difference in the chemical composition of different CSWs, the amount of hydration products varies. Specifically, the alkali-activated CSWs made with CGS have the maximum calcium silicate hydrate (C-S-H), while those prepared with FA enjoy the lowest porosity. In addition, the CO_2 mineralization process will result in the formulation of carbonate and, theoretically, the maximum quantity of mineralized CO_2 is less than 20% of the binder used. Furthermore, compared with CG and CGS, FA is characterized with the highest mineralization capacity. The findings in this study contribute to the understanding of CO_2 mineralization with alkali-activated CSWs.

Keywords: coal-based solid waste; coal mining; backfill; alkali-activated materials; CO_2 mineralization

check for updates

Citation: Huo, B.; Zhang, J.; Li, M.; Zhou, N.; Qiu, X.; Fang, K.; Wang, X. Effect of CO_2 Mineralization on the Composition of Alkali-Activated Backfill Material with Different Coal-Based Solid Wastes. *Sustainability* **2023**, *15*, 4933. https://doi.org/10.3390/su15064933

Academic Editor: Andrea G. Capodaglio

Received: 20 February 2023
Revised: 6 March 2023
Accepted: 8 March 2023
Published: 10 March 2023

1. Introduction

Coal-based solid wastes (CSWs), namely, coal gangue (CG), fly ash (FA), and coal gasification slag (CGS), are emitted in the coal mining and utilization processes. The annual emission of CG, FA, and CGS in China exceeds 680 Mt, 750 Mt, and 100 Mt, respectively [1–3]. The stockpiled CSWs occupy farmland and pollute the soil, water, and the atmosphere [4,5]. Therefore, the utilization of CSWs must be resolved. Backfill mining is an environmental mining technology that offers the advantages of rock strata movement control [6], underground water protection [7], and solid waste utilization [8,9]. Consequently, it has received considerable attention in the research on coal mining.

Carbon dioxide (CO_2) gas, in particular, has the greatest influence on the global climate and is the primary cause of global warming [10,11]. Recently, the growing carbon emissions have posed a formidable challenge both to the coal mining and coal utilization industries [10,11]. Xu et al. [12] reported that a coal mining region will become a zero or negative carbon base in the future. Carbon capture and sequestration in the underground are likely to be the future research directions of coal-based industries. However, underground CO_2 sequestration is still in its infancy, and the research on CO_2 sequestration technologies, equipment, and materials remains incomplete. The most convenient approach is to use backfill pastes as the carrier to sequestrate CO_2 in partitioned confined underground spaces (Figure 1) [13]. Figure 1 shows the schematic of backfill mining combined with CO_2 sequestration. Evidently, after coal mining, a confined space is built in the goaf, and the CO_2 gas transmission pipeline arrayed with different gaps is set in the confined space. Subsequently, the backfill materials are prepared and transported to the confined space through the backfill slurry delivery pipeline. After backfilling and the setting of pastes, the CO_2 gas is transported to the confined space along the pipeline to react with the pastes. This is an ideal treatment approach for underground CO_2 mineralization, which is different to Carbon Capture, Utilization and Storage (CCUS), because using backfill materials to sequestrate CO_2 is safer than CCUS; the explosion of geological storage can lead to the leakage of CO_2 into the atmosphere, and the ground movements might seriously compromise the storage integrity, leading to earthquakes [13].

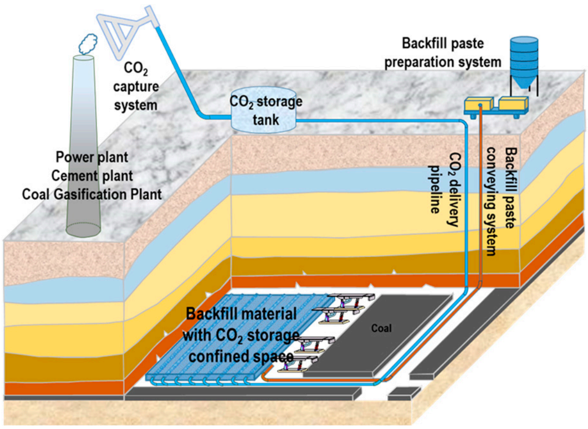

Figure 1. Schematic of CO_2 storage technology for backfill materials in an underground space [13].

The backfill material is the key element for CO_2 sequestration, and the backfill pastes can be prepared with CSWs, such as CG, FA [14,15], and CGS, with minimal cement [16,17] or activators [18,19]. Wang et al. [20] developed a new testing system to investigate the effect of different initial parameters on mineral carbonation, such as initial water-to-binder ratio, sample porosity, and CO_2 pressure. They found that the maximum CO_2 consumption ratio reached 15% within 48 h of carbonation. Chen et al. [21] found that carbonation curing increased the carbonation rate by nearly four times compared with natural curing, and each ton of cemented paste backfill could ideally absorb approximately 78.4 kg of CO_2. It is known that the common chemical compositions of CG, FA, and CGS are CaO, SiO_2, Al_2O_3, and Fe_2O_3 [22,23]; however, their contents differ [24,25]. This results in a difference in their activity levels. Suescum-Morales et al. [26] found that mixes with CO_2 curing and the substitution of FA with MgO resulted in an improvement of CO_2 absorption of 2 g CO_2/kg. The increase in mass due to CO_2 capture was 6.91%, 9.39%, and 12.26% at the ages of 7, 14, and 28 d, respectively, compared to mixes cured with 0.04% (reference) and 5% (CO_2 curing) of CO_2. Miao et al. [27] found that the highest CO_2 adsorption capacity of 2.64 mmol/g at 25 °C was achieved with the acid-treated sample.

Alkali-activated material is an environmentally friendly material without cement and with high solid wastes, which is widely applied in bridge, building and mining [23,28]. The solid wastes consist high amorphous phases that could react with alkali to produce geopolymers/gels [23]. In these solid wastes, FA and slag are the most widely applied materials due to their being easily acquired. Different to FA, CG needs to be calcined at 500–900 °C to transfer the crystal minerals, such as kaolinite ($Al_2O_3 \cdot 2SiO_2 \cdot H_2O$), to amorphous metakaolin ($Al_2O_3 \cdot 2SiO_2$ or AS_2) [22,24,29]. CGS is a new kind of solid waste consisting of crystal and amorphous phases; the crystal phases include quartz and calcite, and the amorphous phases consist of carbon residue and aluminosilicate. CGS has been studied as a supplementary cementitious material [30]. Recently, the CO_2 binding capacity of alkali-activated materials was studied. Nedeljković et al. [28] found that alkali-activated pastes have similar CO_2 binding capacities regardless of the FA/slag ratio. It was observed that the silicate functional groups corresponding to the reaction products in the pastes are progressively changing during the first 7 days. It was also found that the CO_2 bound in the alkali-activated pastes occurs, to a substantial extent, in an amorphous form. The results in Jani and Imqam's [31] experiment indicated that the surface of the FA-based alkali-activated cement cores is not substantively changed after the exposure to CO_2, and no reduction in compressive strength was observed; it was summarized that the FA is hard to react with the CO_2. However, for backfill pastes, the composition and CO_2 mineralized properties of alkali-activated CSWs prepared with different CSWs, especially for alkali-activated CG and CGS, remains unclear.

To address this, the composition and CO_2 mineralization properties of different CSWs used as backfill material was investigated in this study. Backfill pastes prepared with three typical CSWs—CG, FA, and CGS—were employed, with sodium hydroxide as the activator, and their properties were systematically studied using the Gibbs Energy Minimization Software (GEMS). This study can serve as a reference for solid waste recycling and carbon sequestration in the mining industry.

2. Materials and Methods

2.1. Materials

In this study, three types of typical CSWs reported in the literature—CG [29], CGS [30], and FA [31,32]—were used as the raw materials. The chemical compositions of the CG, FA, and CGS were detected by X-ray fluorescence analysis (XRF) according to literatures [30–32] and normalized to 100% (Table 1). These oxides in the raw materials are among the range reported in the previous literature [1–3], showing that they are representative for the CSWs. In addition, sodium hydroxide (NaOH) was selected as the admixture to activate the CSWs.

Table 1. Chemical compositions of CSWs (wt.%).

Material	SiO_2	Al_2O_3	Fe_xO_y	CaO	MgO	K_2O	Na_2O	TiO_2	SO_3
CG	65.50	24.50	3.86	3.04	0.55	1.93	0.62	/	/
FA	41.33	41.55	5.21	8.49	0.49	/	0.69	1.40	0.84
CGS	55.52	17.66	12.24	9.17	2.11	/	/	/	3.30

2.2. Mix Proportion

Table 2 lists the mix proportions of the alkali-activated CSWs in this experiment. The water-to-binder ratio (w/b) of all pastes in the experiment was 0.8. The binder consisted of solid waste and NaOH, and the ratio of NaOH was 0–20% based on the binder. Additionally, to examine the CO_2-mineralized capacity of the binders, the CO_2 addition was set in the range of 0–100% for the pastes.

Table 2. Proportion of the experiment.

Group	Binder Type	Binder Weight/g	Activator/%	CO_2 Dosage/%	w/b
Alkali-activated CG	CG + NaOH	100	0–20	0–100	0.8
Alkali-activated FA	FA + NaOH	100	0–20	0–100	0.8
Alkali-activated CGS	CGS + NaOH	100	0–20	0–100	0.8

2.3. Thermoldynamic Model and Calculation

The GEMS (http://gems.web.psi.ch/, accessed on 17 June 2021. Paul Scherrer Institute, Villigen, Switzerland) [33–35] was used to determine the composition and CO_2 mineralized performance of alkali-activated CSWs. GEMS is a Gibbs Energy Minimization program package for interactive thermodynamic modeling of heterogeneous aquatic (geo)chemical systems, especially those involving metastability and dispersity of mineral phases, solid solution-aqueous solution equilibria, and adsorption/ion exchange.

GEMS described the reactions based on the chemical equilibria theory (e.g., considering gypsum in a glass of water). The primary reaction is described by Equation (1).

$$CaSO_4{\cdot}2H_2O \rightarrow Ca^{2+} + SO_4{}^{2-} + 2H_2O \quad (1)$$

The complex formation solubility products depending on the equilibrium constants are expressed in Equations (2)–(5). Here, the equilibrium constants depend on temperature and pressure.

$$K_{S0} = [Ca^{2+}]{\cdot}[SO_4{}^{2-}] = 10^{-4.58} \quad (2)$$

$$K = [CaOH^{+}]/[Ca^{2+}]{\cdot}[OH^{-}] = 10^{1.22} \quad (3)$$

$$K = [CaSO_4{}^{0}]/[Ca^{2+}]{\cdot}[SO_4{}^{2-}] = 10^{2.3} \quad (4)$$

$$K = [H^{+}]{\cdot}[OH^{-}] = 10^{-14.00} \quad (5)$$

In this experiment, the considered solid solutions of all the cases were modelled in GEMS using the simple ideal mixing model. The environmental temperature and pressure for alkali activation and CO_2 mineralization were 20 °C and 0.1 MPa (1 bar), respectively. The database used in this study was Cemdata18 [36]. Cemdata18 database in GEM can be freely downloaded (http://www.empa.ch/cemdata (accessed on 11 October 2018)) and is fully compatible with the GEMS version. Here, the alkali-activated material (AAM) and deselection of cement (PC) were applied in this software.

The calculated steps of this study are drawn as follows: The CG, FA, and CGS were defined firstly as raw materials in GEMS according to Table 1. The, all the elements necessary to model alkali or carbonation reactions, including H, C, N, O, Na, Mg, Al, Si, S, Cl, K, Ca and Fe, were selected. The activity and ionic strength of the ions, such as Ca^{2+}, were calculated with reference to the extended Debye–Hückel model (Equations (6)–(8)). After that, the mix proportions for the pastes (Table 2) were input into GEMS and the reactions were performed.

$$\log \gamma = \frac{-AZ^2\sqrt{I}}{1 + Ba\sqrt{I}} + bI \quad (6)$$

where γ is the activity coefficient, A and B are P, T is dependent coefficients, a is an average distance of approach of two ions of opposite charge (or the ion-size Kielland's parameter for individual ions), b is a semi-empirical parameter (~0.123 for KOH and ~0.098 for NaOH electrolyte at 25 °C), I is the effective molal ionic strength, and

$$A = 1.82483 * 10^6 \rho_0^{0.5} (\varepsilon_0 \cdot T)^{-1.5} \quad (7)$$

$$B = 50.2916 \rho_0^{0.5} (\varepsilon_0 \cdot T)^{-1.5} \quad (8)$$

where ρ_0 is density ($g{\cdot}cm^{-3}$) and ε_0 is the dielectric constant of pure water at the temperature T (K) and pressure P (bar) of interest.

From the solubility products, K, of solids calculated at different temperatures, T, the Gibbs free energy of reaction, $\Delta_r G^0$, the Gibbs free energy of formation, $\Delta_f G^0$, and the absolute entropy, S^0, at T_0 = 298.15 K were obtained according to Equations (9) and (10).

$$\Delta_r G^{0^0} = \sum_i v_i \Delta_f G^0 = -RT \ln K \quad (9)$$

$$\Delta_a G_T^0 = \Delta_f G_{T_0}^0 - S_{T_0}^0 (T - T_0) + \int_{T_0}^{T} C_p^0 dT - \int_{T_0}^{T} \frac{C_p^0}{T} dT \quad (10)$$

where v_i are the stoichiometric reaction coefficients, R = 8.31451 J/mol/K, T is the temperature in K, and C_p^0 is the heat capacity at constant pressure. The apparent Gibbs free energy of formation, $\Delta_a G_T^0$, refers to standard Gibbs energies of elements at 298.15 K.

Additionally, the aqua in the pastes which could be recognized as the pore was calculated by GEMS.

3. Results and Discussion

3.1. Composition of Alkali-Activated CSWs

Composition is fundamental to alkali-activated CSWs, and significantly affects their properties [16,19]. Figures 2–4 show the compositions of alkali-activated CG, FA, and CGS pastes with different amounts of NaOH after the completion of all chemical reactions. As is evident from Figure 2, alkali-activated CSWs are primarily composed of calcium silicate hydrate (C-S-H), magnesium silicate hydrate (M-S-H), kaolinite, goethite, natrolite, quartz, and liquid. With increased NaOH addition, the kaolinite reacts with NaOH to produce natrolite. The reaction is described by Equation (11). When the NaOH content reaches 20 wt.%, the kaolinite in the CG is completely consumed.

$$Al_2O_3{\cdot}2SiO_2 + SiO_2 + NaOH \rightarrow Na_2Al_2Si_3O_{10}{\cdot}2H_2O \tag{11}$$

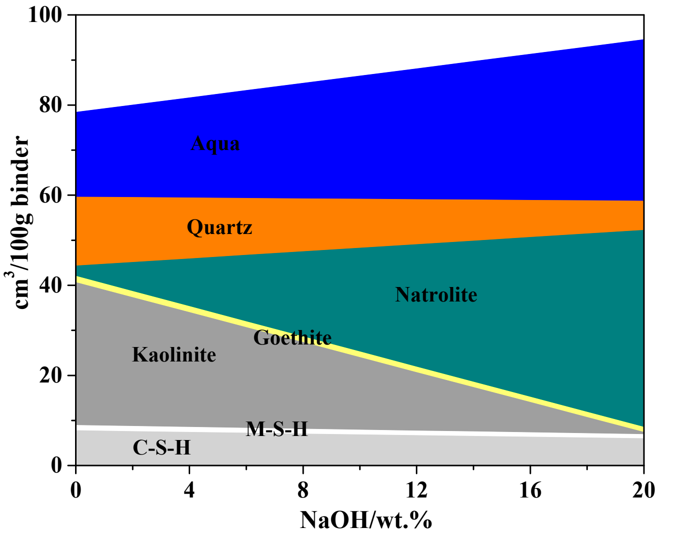

Figure 2. Effect of NaOH dosage on the composition of alkali-activated CG.

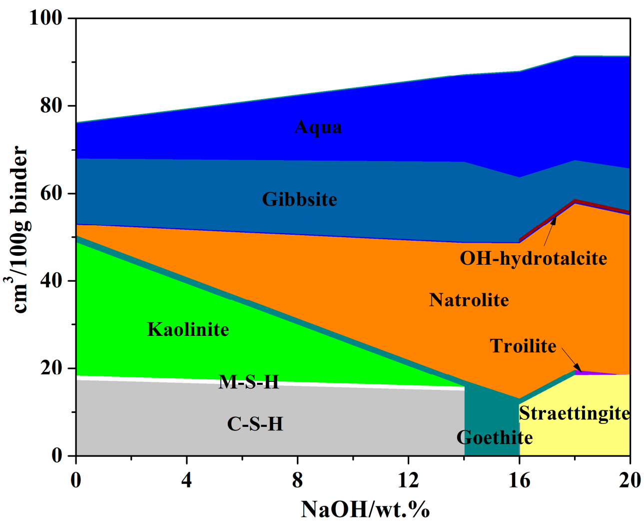

Figure 3. Effect of NaOH dosage on the composition of alkali-activated FA.

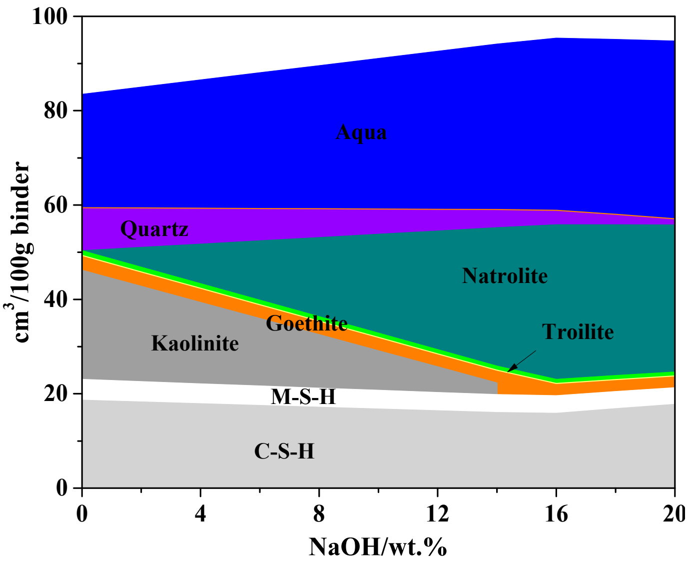

Figure 4. Effect of NaOH dosage on the composition of alkali-activated CGS.

Figure 3 shows the compositions of alkali-activated FA with additions of different amounts of NaOH. Compared with alkali-activated CG, except for C-S-H, M-S-H, kaolinite, goethite, and natrolite, alkali-activated FA contains additional hydrates, such as gibbsite, staettingite, troilite, and OH-hydrotalcite, because of the higher Al content in FA than CG. The hydrates in the CGS activated by NaOH contain more C-S-H gel and Trollite, as shown in Figure 4. This is because CGS has higher CaO and Fe_2O_3 content than CG and FA, as shown in Table 1.

However, in practical applications, FA and CGS typically have a higher content of amorphous phases, which are excellent raw minerals for alkali activation. While CG includes kaolinite, quartz, and calcite, these phases are difficult to be activated in alkali. Therefore, FA and CGS are more suitable raw materials for alkali-activated CSWs than CG. However, the thermal activated CG is good material for alkali activation; this is because the high content of clay mineral in gangue is found to be a potential source of pozzolan, while proper activation is needed to improve the pozzolanic reactivity of gangue due to its relatively stable (crystalline) chemical structure. The metakaolin formed after thermal activation is an amorphous mineral demonstrating excellent pozzolanic properties (Equation (12)), containing silica and alumina in an active form which can react with calcium hydroxide (CH) or NaOH derived from cement hydration or alkali activation [22,24,29].

$$Al_2O_3{\cdot}2SiO_2{\cdot}2H_2O \xrightarrow{500-900\ ^\circ C} Al_2O_3{\cdot}2SiO_2 + 2H_2O(g) \tag{12}$$

The compressive strength property of alkali-activated materials depends on their mineral compositions and pore structure [29,32]. Higher C-S-H and lower pore content result in better compressive strength. In addition, several studies [37,38] have reported that the optimum Na_2O (chemical expression of the alkali activator) amount based on the binder is 4%. To compare the compositions of the three types of alkali-activated CSWs, 8 wt.% NaOH was added to activate the alkali-activated CSWs. The quantitative composition results of alkali-activated CSWs are presented in Table 3. The cementitious hydrates, including C-S-H, M-S-H, and natrolite, in alkali-activated CG, FA, and CGS reached 26.95 cm^3/100 g, 35.80 cm^3/100 g, and 37.93 cm^3/100 g, respectively, while the total pore content was 25.62 cm^3/100 g, 14.99 cm^3/100 g, and 30.31 cm^3/100 g, respectively. The higher the hydrate content and the lower the porosity, the better the mechanical and permeability properties of cementitious materials. Although the hydrate content of alkali-activated FA and CGS is almost identical, the porosity of alkali-activated FA is significantly lower than that of alkali-activated CGS. Among the three pastes, the cementitious hydrate content of the alkali-activated CG is the lowest. Therefore, for the same amount of alkali activator, the performance of alkali-activated FA is better. This result is consistent with those reported in previous studies using FA as the alkali-activated raw material [4,15,23].

Table 3. Compositions (cm^3/100 g) of the alkali-activated CSWs with 8 wt.% NaOH.

Mineral	Alkali-Activated CG	Alkali-Activated FA	Alkali-Activated CGS
C-S-H	6.98	15.77	17.13
M-S-H	1.09	0.95	4.05
Kaolinite	19.20	13.13	11.35
Goethite	1.28	1.42	2.88
Troilite	0.01	0.24	0.93
Natrolite	18.88	19.08	16.75
Quartz	11.75	/	6.12
Gibbsite	/	16.84	/
Pore	25.62	14.99	30.31

3.2. CO_2-Mineralization Property of Alkali-Activated CSWs

C-S-H and M-S-H phases have a variable composition that depends on the prevailing Ca/Si and Mg/Si ratios in the system that can change by CO_2 mineralization/carbonation, pozzolanic reaction, leaching caused by the ingress of water, and/or chemical attack. The CO_2-mineralization alters the compositions of the materials, and thus changes the properties alkali-activated materials. To further compare the CO_2 mineralization performance of the three types of alkali-activated CSWs, the effect of CO_2 dosage, ranging from 0% to 100% based on the binder, was systematically investigated. The results are presented in Figures 5–7.

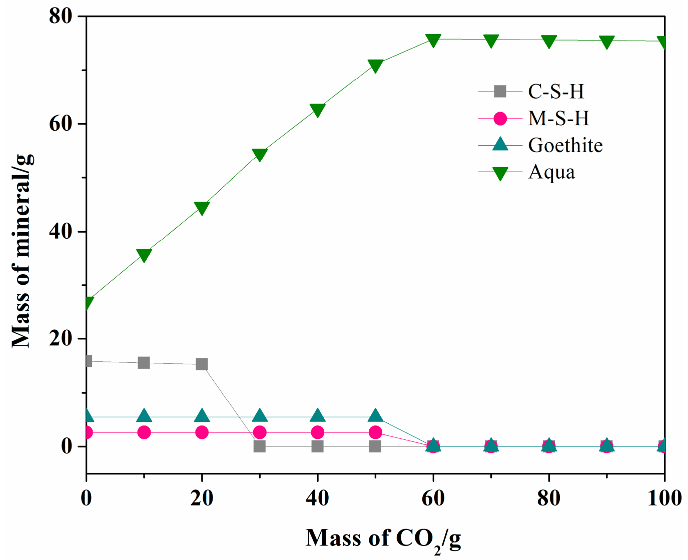

Figure 5. Effect of CO_2 addition on the composition of alkali-activated CG.

As shown in Figure 5, with an increase in CO_2, C-S-H, M-S-H, goethite reacts with CO_2, and its content decreases. The reactions are expressed in Equations (13)–(15). CO_2 mineralization leads to the accelerated removal of Ca/Mg element from the C-S-H/M-S-H gels, resulting in a lower Ca/Si and Mg/Si ratio of the gel and a degradation of the stability of C-S-H/M-S-H. These carbonation reactions produce a large amount of water, resulting in an increase in the liquid phase. It is found that sodium zeolite cannot be carbonated, as its chemical composition is $Na_2Al_2Si_3O_{10}\cdot 2H_2O$, in which no Ca and Mg elements are found. In addition, when the CO_2 addition exceeds 20%, C-S-H in alkali-activated CG decreases rapidly. When the CO_2 addition reaches 30%, the C-S-H gel disappears. M-S-H and goethite can also be carbonated. When the CO_2 addition exceeds 60%, all the minerals that can be carbonated react, causing the carbonation to cease and the liquid phase content dose to remain constant. It is worth noting that C-S-H and M-S-H gel are the key elements that provide mechanical and durability properties [39,40]. This result reveals that CO_2 addition should not exceed 20 wt.%

$$(CaO)_a(SiO_2)_b(H_2O)_c + CO_2 \rightarrow CaCO_3 + SiO_2 + H_2O \quad (13)$$

$$(MgO)_d(SiO_2)_e(H_2O)_f + CO_2 \rightarrow MgCO_3 + SiO_2 + H_2O \quad (14)$$

$$FeO(OH){\cdot}nH_2O + CO_2 \rightarrow Fe_2(CO_3)_3 + H_2O \quad (15)$$

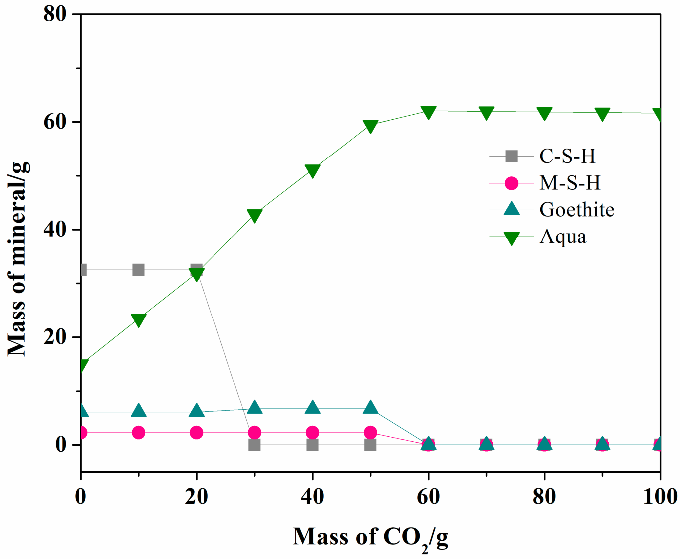

Figure 6. Effect of CO_2 addition on the composition of alkali-activated FA.

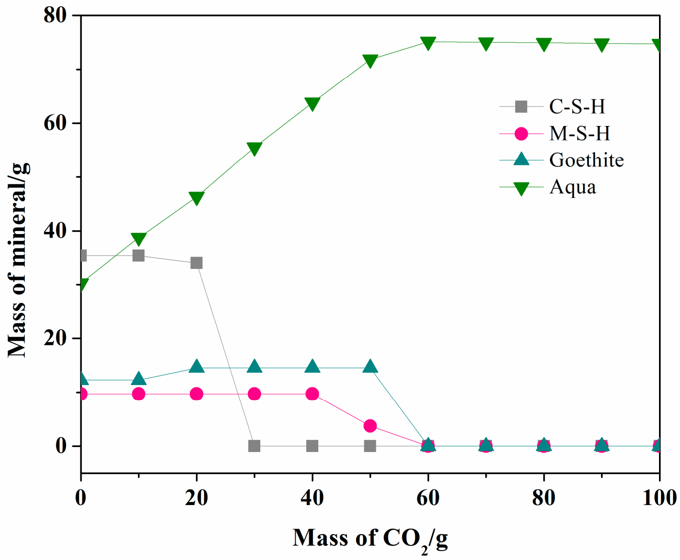

Figure 7. Effect of CO_2 addition on the composition of alkali-activated CGS.

As shown in Figure 6, with increasing CO_2 addition, the reaction of CO_2 with alkali-activated FA is similar to that with alkali-activated CG, while the initial C-S-H content differs due to the higher CaO content in FA. Moreover, the liquid content in alkali-activated FA is lower than that in the alkali-activated CG group, as the liquid phase (aqua) can be recognized as a pore which decreases the compressive strength of materials; it indicates that the compressive strength of alkali-activated FA is better. The initial C-S-H gel content in alkali-activated CGS is the highest among the three types of pastes, as shown in Figure 7.

In addition, the liquid volume in alkali-activated CGS is much higher than that in alkali-activated FA, which is consistent with the experimental results presented in Section 3.1.

From the above reactions, it is evident that the carbonation reactions result in the decrease of cementitious hydrates and increase of calcite and liquid. As reported in the previous work [16,20,21], the effects of CO_2 mineralization on the microstructure and compressive strength are depending on their reaction degree, which can be divided into two stages. At the initial CO_2 mineralized stage, the calcite and magnesium carbonate produced in the reactions act as fillers to fill the pores in the cementitious matrix, resulting in a decrease in the pore content and an increase in the compressive strength; while at the later stage, most of the C-S-H or M-S-H are carbonated by the CO_2; this finding provides support for the degeneration of microstructure and strength of the matrix [41] (as shown in Figure 8). Thus, the carbonation in the alkali-activated CSWs should be precisely controlled based on its mineral compositions and microstructure. Otherwise, the insufficient compressive strength of the backfill materials struggles to control the movement of strata.

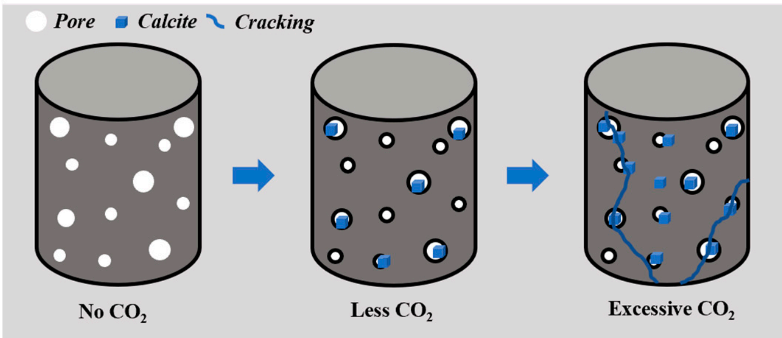

Figure 8. Schematic diagram of the effect of CO_2 mineralization on the structure of cement pastes under different conditions.

3.3. Effect of CO_2 Mineralization on the Volume of Alkali-Activated CSWs

CO_2 mineralization involves chemical reactions that carbonate hydrates in the presence of CO_2, resulting in a solid volume change. The volume change of the cementitious materials is a serious problem, especially in the alkali-activated materials, such as shrinkage and expansion [22,23,26]. Shrinkage or expansion is considered as a free dimensional change without external loading, which can cause cracking in the paste or at the paste/aggregate interface under restrained condition. To examine the impact of CO_2 sequestration on solid volume changes in alkali-activated CSWs, comparisons were performed with the same NaOH addition. Further, the effect of CO_2 addition, ranging from 0–100%, was examined based on the binder.

As shown in Figure 9, with an increase in CO_2, the volume of the three types of alkali-activated CSWs initially decreases, then increases, and finally stabilizes. This is because C-S-H, M-S-H, and goethite initially react with CO_2 to produce carbonated products and water. In this process, the solid volume of the product increases, resulting in a decrease in the solid volume of the alkali-activated CSWs. When the C-S-H gel is carbonated, the solid phase volume reaches the lowest point. Subsequently, the solid phase volume increases, and the carbonated volume of M-S-H and goethite increases. The solid phase volume content then increases until all hydrated products are carbonated, and the solid phase volume remains constant. Comparing the solid phase volume content of the three types of alkali-activated CSWs reveals that the order of volume content is alkali-activated FA > CG > CGS, which is consistent with the experimental results presented in Section 3.1.

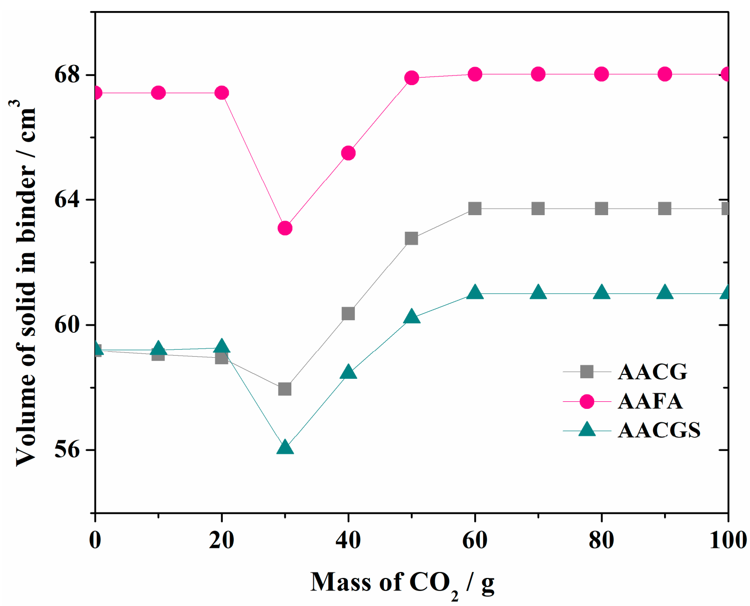

Figure 9. Effect of CO_2 addition on the volume of alkali-activated CSWs.

3.4. CO_2 Sequestrated Potential of CSWs in Underground Space

The underground space backfilled with solid wastes to mineralize CO_2 is considered to be a potential future substitute for carbon capture, utilization, and storage (CCUS). CO_2 mineralization is safer than the geological storage facility in that in the geological storage facility, there might be sudden blowouts or explosions leading to a leakage of CO_2 into the atmosphere, or the ground movements might seriously compromise the storage integrity, leading to earthquakes. However, the underground space for CO_2 sequestration is unclear. It is estimated that the underground space in the goaf will reach 23.452 billion m^3 by 2030 [42]. This indicates the potential to explore underground space in the future. To examine the suitability of the underground space for disposing and utilizing CSWs and CO_2, three types of solid wastes were compared based on the results presented in this section, and the proportions in Table 4 were selected. The results are presented in Figure 10.

Table 4. Proportion of alkali-activated CSWs for backfill and CO_2 storage.

Material	Solid Waste/g	NaOH/g	Water/g	Volume of Binder/cm^3	CO_2 Storage on Binder/%
Alkali-activated CG	CG-92	8	80	84.80	20
Alkali-activated FA	AA-92	8	80	82.42	20
Alkali-activated CGS	CGS-92	8	80	89.52	20

As shown in Figure 10, if the underground space is fully backfilled with solid waste, the theoretical utilization of CG, FA, and CGS can reach 254 × 10^8 t, 262 × 10^8 t, and 241 × 10^8 t, respectively, and the theoretical CO_2 storage can reach 55 × 10^8 t, 57 × 10^8 t, and 52 × 10^8 t, respectively. This will have a significant frontal impact on the environment. However, the actual CO_2 sequestration efficiency is generally much lower than the theoretical value, which mainly depends on the material properties, such as particle size and composition, or process parameters, such as temperature and pressure. Previous studies [16,26,27] have found that the actual CO_2 storage efficiency can exceed 10% of the theoretical values; therefore, the potential utilization of CO_2 is still appreciable.

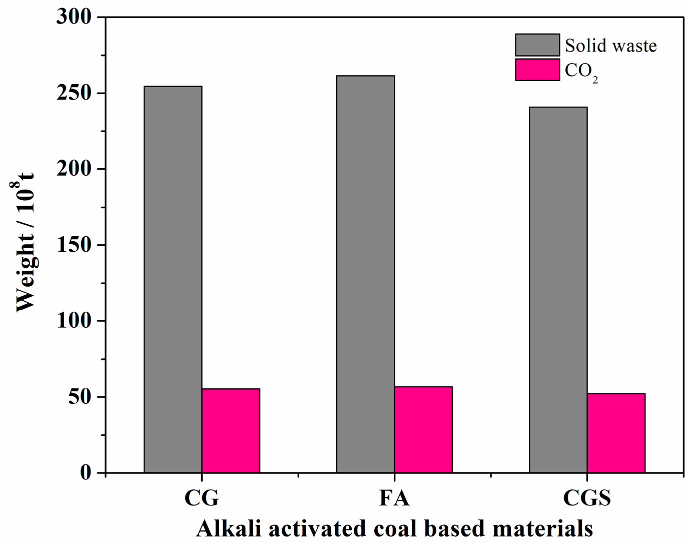

Figure 10. Consumption of alkali-activated CSWs and CO_2 storage.

4. Conclusions

In this study, the composition and CO_2 mineralization of alkali-activated CG, FA, and CGS were comprehensively investigated by GEMS. The following conclusions were drawn.

(1) The hydration products of alkali-activated CG, FA, and CGS are calcium silicate hydrate (C-S-H), magnesium silicate hydrate (M-S-H), kaolinite, goethite, natrolite, and liquid. Alkali-activated FA also produces gibbsite, troilite, and OH hydrotalcite because of the different chemical compositions;

(2) The cementitious hydrate content in alkali-activated FA and CGS is almost identical; however, the porosity of alkali-activated FA is significantly lower than that of alkali-activated CGS, and the cementitious hydrate content in alkali-activated CG is the lowest. For the same amount of NaOH, alkali-activated FA offers superior performance;

(3) Hydrates, such as C-S-H, M-S-H, and goethite, can easily be carbonated to produce carbonates and water. The carbonization reaction results in volume changes in the pastes. The maximum theoretical CO_2 sequestration capacity should be less than 20% based on the pastes; otherwise, the backfill materials will be destroyed;

(4) CG, FA, and CGS have a high potential for use as backfill materials in underground space and in CO_2 sequestration. In particular, FA offers superior performance.

This study provides a comprehensive chemical understanding of the effect of CO_2 mineralization on the composition of alkali-activated CSWs with different coal-based solid wastes. The strength and volume change properties of alkali-activated CSWs in application, however, need to be studied in future work.

Author Contributions: Conceptualization, B.H. and J.Z.; methodology, B.H., K.F. and M.L.; formal analysis, B.H.; investigation, B.H.; data curation, B.H., M.L. and X.Q.; writing—original draft preparation, B.H.; writing—review and editing, B.H., N.Z., X.W. and X.Q.; supervision, J.Z. and K.F.; project administration, B.H. and J.Z.; funding acquisition, B.H., M.L. and J.Z. All authors have read and agreed to the published version of the manuscript.

Funding: This research was financially supported by the Jiangsu Funding Program for Excellent Postdoctoral Talent (2022ZB524), the Fundamental Research Funds for the Central Universities (2022QN1007), the National Natural Science Foundation of China (52130402 and 52004271) and the Project of China National Coal Group Co., Ltd. (2022JB02).

Institutional Review Board Statement: Not applicable.

Informed Consent Statement: Not applicable.

Data Availability Statement: Data are contained within the article.

Acknowledgments: The authors acknowledge the China University of Mining and Technology (CUMT) for providing the experimental platform, and the reviewers for their scientific comments and suggestions. The authors are grateful to Jixiong Zhang and Nan Zhou for their instructions on topic selection, Meng Li for kindly providing the materials, and Kun Fang for their help in the experiments.

Conflicts of Interest: The authors declare no conflict of interest.

Abbreviations

CSW	Coal-based solid waste
CG	coal gangue
FA	fly ash
CGS	coal gasification slag
GEMS	Gibbs Energy Minimization Software

References

1. Zhang, Y.L.; Ling, T.C. Reactivity Activation of Waste Coal Gangue and Its Impact on the Properties of Cement-Based Materials—A Review. *Constr. Build. Mater.* **2020**, *234*, 117424. [CrossRef]
2. Li, Z.; Xu, G.; Shi, X. Reactivity of Coal Fly Ash Used in Cementitious Binder Systems: A State-of-the-Art Overview. *Fuel* **2021**, *301*, 121031. [CrossRef]
3. Miao, Z.; Guo, Z.; Qiu, G.; Jia, W.; Jiao, K.; Zhang, Y.; Wu, J. Insight into the Role of Slag Particles in Coal Gasification Fine Slag on Hierarchical Porous Composites Preparation and CO_2 Capture. *Fuel* **2022**, *310*, 122475. [CrossRef]
4. Tang, Q.; Zhang, H.; Zhao, X.; Miao, C.; Yang, P.; Zhou, Z.; Ji, Q.; Chen, L. Speciation, Bioaccessibility and Human Health Risk Assessment of Chromium in Solid Wastes from an Ultra-Low Emission Coal-Fired Power Plant, China. *Environ. Pollut.* **2022**, *315*, 120400. [CrossRef] [PubMed]
5. Wang, C.; Duan, D.; Huang, D.; Chen, Q.; Tu, M.; Wu, K.; Wang, D. Lightweight Ceramsite Made of Recycled Waste Coal Gangue & Municipal Sludge: Particular Heavy Metals, Physical Performance and Human Health. *J. Clean. Prod.* **2022**, *376*, 134309.
6. Zhou, N.; Du, E.; Zhang, J.; Zhu, C.; Zhou, H. Mechanical Properties Improvement of Sand-Based Cemented Backfill Body by Adding Glass Fibers of Different Lengths and Ratios. *Constr. Build. Mater.* **2021**, *280*, 122408. [CrossRef]
7. Zhang, Q.; Zhang, J.X.; Wu, Z.Y.; Chen, Y. Overview of Solid Backfilling Technology Based on Coal-Waste Underground Separation in China. *Sustainability* **2019**, *11*, 2118. [CrossRef]
8. Xue, G.L.; Yilmaz, E.; Song, W.D.; Cao, S. Compressive Strength Characteristics of Cemented Tailings Backfill with Alkali-Activated Slag. *Appl. Sci.* **2018**, *8*, 1537. [CrossRef]
9. Hu, J.H.; Ding, X.T.; Ren, Q.F.; Luo, Z.Q.; Jiang, Q. Effect of Incorporating Waste Limestone Powder into Solid Waste Cemented Paste Backfill Material. *Appl. Sci.* **2019**, *9*, 2076. [CrossRef]
10. Wang, W.; Hu, Y.; Lu, Y. Driving Forces of China's Provincial Bilateral Carbon Emissions and the Redefinition of Corresponding Responsibilities. *Sci. Total Environ.* **2023**, *857*, 159404. [CrossRef]
11. Dogan, E.; Turkekul, B. CO_2 Emissions, Real Output, Energy Consumption, Trade, Urbanization and Financial Development: Testing the EKC Hypothesis for the USA. *Environ. Sci. Pollut. Res.* **2016**, *23*, 1203–1213. [CrossRef] [PubMed]
12. Xu, J.; Dai, J.; Xie, H.; Lv, C. Coal Utilization Eco-Paradigm towards an Integrated Energy System. *Energy Policy* **2017**, *109*, 370–381. [CrossRef]
13. Li, K. *Diffusion and Adsorption Study of CO_2 in Mined out Areas of Coal Mines Filled with Coal Gangue Materials*; China University of Mining and Technology: Xuzhou, China, 2021.
14. Shi, X.; Wang, X.; Wang, X. Dual Waste Utilization in Cemented Paste Backfill Using Steel Slag and Mine Tailings and the Heavy Metals Immobilization Effects. *Powder Technol.* **2022**, *403*, 117413. [CrossRef]
15. Li, M.; Zhang, J.; Li, A.; Zhou, N. Reutilisation of Coal Gangue and Fly Ash as Underground Backfill Materials for Surface Subsidence Control. *J. Clean. Prod.* **2020**, *254*, 120113. [CrossRef]
16. Wang, X.; Ni, W.; Li, J.; Zhang, S.; Hitch, M.; Pascual, R. Carbonation of Steel Slag and Gypsum for Building Materials and Associated Reaction Mechanisms. *Cem. Concr. Res.* **2019**, *125*, 105893. [CrossRef]
17. Zaibo, Z.; Juanhong, L.; Aixiang, W.; Hongjiang, W. Coupled Effects of Superplasticizers and Glazed Hollow Beads on the Fluidy Performance of Cemented Paste Backfill Containing Alkali-Activated Slag and MSWI Fly Ash. *Powder Technol.* **2022**, *399*, 116726. [CrossRef]
18. Behera, S.K.; Mishra, D.P.; Singh, P.; Mishra, K.; Mandal, S.K.; Ghosh, C.N.; Kumar, R.; Mandal, P.K. Utilization of Mill Tailings, Fly Ash and Slag as Mine Paste Backfill Material: Review and Future Perspective. *Constr. Build. Mater.* **2021**, *309*, 125120. [CrossRef]
19. Jiang, H.; Ren, L.; Zhang, Q.; Zheng, J.; Cui, L. Strength and Microstructural Evolution of Alkali-Activated Slag-Based Cemented Paste Backfill: Coupled Effects of Activator Composition and Temperature. *Powder Technol.* **2022**, *401*, 117322. [CrossRef]
20. Wang, P.; Mao, X.; Chen, S.-E. CO_2 Sequestration Characteristics in the Cementitious Material Based on Gangue Backfilling Mining Method. *Int. J. Min. Sci. Technol.* **2019**, *29*, 721–729. [CrossRef]

21. Chen, Q.; Zhu, L.; Wang, Y.; Chen, J.; Qi, C. The Carbon Uptake and Mechanical Property of Cemented Paste Backfill Carbonation Curing for Low Concentration of CO_2. *Sci. Total Environ.* **2022**, *852*, 158516. [CrossRef]
22. Shao, S.; Ma, B.; Wang, C.; Chen, Y. Thermal Behavior and Chemical Reactivity of Coal Gangue during Pyrolysis and Combustion. *Fuel* **2023**, *331*, 125927. [CrossRef]
23. Giergiczny, Z. Fly Ash and Slag. *Cem. Concr. Res.* **2019**, *124*, 105826. [CrossRef]
24. Liu, X.; Jin, Z.; Jing, Y.; Fan, P.; Qi, Z.; Bao, W.; Wang, J.; Yan, X.; Lv, P.; Dong, L. Review of the Characteristics and Graded Utilisation of Coal Gasification Slag. *Chin. J. Chem. Eng.* **2021**, *35*, 92–106. [CrossRef]
25. Lee, Y.-R.; Soe, J.T.; Zhang, S.; Ahn, J.-W.; Park, M.B.; Ahn, W.-S. Synthesis of Nanoporous Materials via Recycling Coal Fly Ash and Other Solid Wastes: A Mini Review. *Chem. Eng. J.* **2017**, *317*, 821–843. [CrossRef]
26. Suescum-Morales, D.; Bravo, M.; Silva, R.V.; Jiménez, J.R.; Fernandez-Rodriguez, J.M.; de Brito, J. Effect of Reactive Magnesium Oxide in Alkali-Activated Fly Ash Mortars Exposed to Accelerated CO_2 Curing. *Constr. Build. Mater.* **2022**, *342*, 127999. [CrossRef]
27. Miao, Z.; Xu, J.; Chen, L.; Wang, R.; Zhang, Y.; Wu, J. Hierarchical Porous Composites Derived from Coal Gasification Fine Slag for CO_2 Capture: Role of Slag Particles in the Composites. *Fuel* **2022**, *309*, 122334. [CrossRef]
28. Nedeljković, M.; Ghiassi, B.; Melzer, S.; Kooij, C.; van der Laan, S.; Ye, G. CO_2 binding capacity of alkali-activated fly ash and slag pastes. *Ceram. Int.* **2018**, *44*, 19646–19660. [CrossRef]
29. Zhang, W.; Chai, J.; Feng, X.; Dong, C.; Sun, Q.; Li, M.; Wang, L. Preparation and microstructure of coal gangue-based geopolymer. *J. China Univ. Min. Technol.* **2021**, *50*, 539–547.
30. Gu, Y.; Wang, D.; Fang, K.; Yao, G.; Wang, Q.; Zhang, M.; Sun, R.; Lv, N. Dissolution Characteristics of Coal Gasification Slag and Its Effect on Cement-Based Materials. *Bull. Chin. Ceram. Soc.* **2021**, *40*, 1579–1585.
31. Jani, P.; Imqam, A. Class C fly ash-based alkali activated cement as a potential alternative cement for CO_2 storage applications. *J. Pet. Sci. Eng.* **2021**, *201*, 108408. [CrossRef]
32. Wang, J.; Huang, T.; Cheng, G.; Liu, Z.; Li, S.; Wang, D. Effects of Fly Ash on the Properties and Microstructure of Alkali-Activated FA/BFS Repairing Mortar. *Fuel* **2019**, *256*, 115919. [CrossRef]
33. Kulik, D.; Wagner, T.; Dmytrieva, S.; Kosakowski, G.; Hingerl, F.; Chudnenko, K.; Berner, U. GEM-Selektor geochemical modeling package: Revised algorithm and GEMS3K numerical kernel for coupled simulation codes. *Computat. Geosci.* **2013**, *17*, 1–24. [CrossRef]
34. Wagner, T.; Kulik, D.; Hingerl, F.; Dmytrieva, S. GEM-Selektor geochemical modeling package: TSolMod library and data interface for multicomponent phase models. *Can. Mineral.* **2012**, *50*, 1173–1195. [CrossRef]
35. Thoenen, T.; Kulik, D. *Nagra/PSI Chemical Thermodynamic Data Base 01/01 for the GEM-Selektor (V.2-PSI) Geochemical Modeling Code: Release 28-02-03*; Internal Report TM-44-03-04; Paul Scherrer Institute: Villigen, Switzerland, 2003. Available online: http://gems.web.psi.ch/TDB/doc/pdf/TM-44-03-04-web.pdf (accessed on 28 February 2003).
36. Lothenbach, B.; Kulik, D.A.; Matschei, T.; Balonis, M.; Baquerizo, L.; Dilnesa, B.; Miron, G.D.; Myers, R.J. Cemdata18: A Chemical Thermodynamic Database for Hydrated Portland Cements and Alkali-Activated Materials. *Cem. Concr. Res.* **2019**, *115*, 472–506. [CrossRef]
37. You, N.; Shi, J.; Zhang, Y. Corrosion Behaviour of Low-Carbon Steel Reinforcement in Alkali-Activated Slag-Steel Slag and Portland Cement-Based Mortars under Simulated Marine Environment. *Corros. Sci.* **2020**, *175*, 108874. [CrossRef]
38. Li, N.; Farzadnia, N.; Shi, C. Microstructural Changes in Alkali-Activated Slag Mortars Induced by Accelerated Carbonation. *Cem. Concr. Res.* **2017**, *100*, 214–226. [CrossRef]
39. Gallucci, E.; Zhang, X.; Scrivener, K. Effect of temperature on the microstructure of calcium silicate hydrate (CSH). *Cem. Concr. Res.* **2013**, *53*, 185–195. [CrossRef]
40. Zhang, T.; Vandeperre, L.; Cheeseman, C. Formation of magnesium silicate hydrate (MSH) cement pastes using sodium hexametaphosphate. *Cem. Concr. Res.* **2014**, *65*, 8–14. [CrossRef]
41. Zhang, X.; Zheng, Y.; Guo, Z.; Ma, Y.; Wang, Y.; Gu, T.; Yang, T.; Jiao, L.; Liu, K.; Hu, Z. Effect of CO_2 solution on Portland cement paste under flowing, migration, and static conditions. *J. Nat. Gas. Sci. Eng.* **2021**, *95*, 104179. [CrossRef]
42. Xie, H.; Gao, M.; Liu, J.; Zhou, H.; Zhang, R.; Chen, P.; Liu, Z.; Zhang, A. Research on exploitation and volume estimation of underground space in coal mines. *J. China Coal Soc.* **2018**, *43*, 1487–1503.